EC
Journals.ASM.org

A Flucytosine-Responsive Mbp1/Swi4-Like Protein, Mbs1, Plays Pleiotropic Roles in Antifungal Drug Resistance, Stress Response, and Virulence of *Cryptococcus neoformans*

Min-Hee Song,[a] Jang-Won Lee,[a] Min Su Kim,[a] Ja-Kyung Yoon,[a] Theodore C. White,[b] Anna Floyd,[c] Joseph Heitman,[c] Anna K. Strain,[d] Judith N. Nielsen,[e] Kirsten Nielsen,[d] and Yong-Sun Bahn[a]

Department of Biotechnology, Center for Fungal Pathogenesis, College of Life Science and Biotechnology, Yonsei University, Seoul, South Korea[a]; Cell Biology and Biophysics Division, School of Biological Sciences, University of Missouri, Kansas City, Kansas City, Missouri, USA[b]; Departments of Molecular Genetics and Microbiology, Medicine, and Pharmacology and Cancer Biology, Duke University Medical Center, Durham, North Carolina, USA[c]; Department of Microbiology, Medical School, University of Minnesota, Minneapolis, Minnesota, USA[d]; and Department of Pathology and Laboratory Medicine, Division of Laboratory Animal Medicine, University of North Carolina, Chapel Hill, North Carolina, USA[e]

Cryptococcosis, caused by the basidiomycetous fungus *Cryptococcus neoformans*, is responsible for more than 600,000 deaths annually in AIDS patients. Flucytosine is one of the most commonly used antifungal drugs for its treatment, but its resistance and regulatory mechanisms have never been investigated at the genome scale in *C. neoformans*. In the present study, we performed comparative transcriptome analysis by employing two-component system mutants (*tco1*Δ and *tco2*Δ) exhibiting opposing flucytosine susceptibility. As a result, a total of 177 flucytosine-responsive genes were identified, and many of them were found to be regulated by Tco1 or Tco2. Among these, we discovered an APSES-like transcription factor, Mbs1 (Mbp1- and Swi4-like protein 1). Expression analysis revealed that *MBS1* was regulated in response to flucytosine in a Tco2/Hog1-dependent manner. Supporting this, *C. neoformans* with the deletion of *MBS1* exhibited increased susceptibility to flucytosine. Intriguingly, Mbs1 played pleiotropic roles in diverse cellular processes of *C. neoformans*. Mbs1 positively regulated ergosterol biosynthesis and thereby affected polyene and azole drug susceptibility. Mbs1 was also involved in genotoxic and oxidative stress responses. Furthermore, Mbs1 promoted production of melanin and capsule and thereby was required for full virulence of *C. neoformans*. In conclusion, Mbs1 is considered to be a novel antifungal therapeutic target for treatment of cryptococcosis.

Cryptococcus neoformans is a basidiomycetous fungus that has both saprobic and parasitic life cycles. In the natural environment, including soil, trees, and pigeon guano, *C. neoformans* exists as both yeast and filamentous forms and undergoes sexual differentiation with cells of the opposite mating type (*MAT*α and *MAT***a** cells) and monokaryotic fruiting with the same mating type. Upon inhalation of its dried yeast form or basidiospores through the respiratory tract, a susceptible host may develop fungal pneumonia and fatal meningoencephalitis by subsequent dissemination of the pathogen, particularly to the central nervous system (CNS) (24, 34). A recent retrospective epidemiological study shows that approximately 957,000 cases of HIV/AIDS-related cryptococcal meningitis, which result in more than 600,000 deaths within 3 months after infection, occur annually worldwide (46). However, cryptococcal meningitis is not limited to just the immunocompromised populations, as witnessed by the emergence of *Cryptococcus gattii* in the Pacific Northwest region of Canada and the United States since 1999 (16), which has caused fatal diseases in immunocompetent individuals.

Despite global concerns, only a limited number of antifungal agents, such as amphotericin B (AMB), flucytosine, and azole drugs, are clinically available for treatment of cryptococcosis. Unfortunately, these antifungal drugs have inherent problems, such as toxicity to multiple organs, including liver and kidney, and the emergence of resistant strains (3, 4, 9, 52). The narrow option of available antifungal drugs led researchers not only to aim to develop novel antifungal targets but also to attempt various combination therapies to yield synergistic antifungal effects. The major advantages of combination antifungal therapy include reduction of the dose and toxicity inherent to each drug, potential decrease in the number of drug-resistant strains, and broadening of the antifungal spectrum (3, 39, 49). Several fungal signaling pathways have been recognized to be potentially good targets for development of combination therapy with azole or polyene drugs with synergistic anticryptococcal effects (14, 18, 27, 29, 32, 40). In contrast, targets for combination therapy with flucytosine are relatively poorly known. Flucytosine, a fluorinated analogue of cytosine, is known to be effective in treatment of candidiasis and cryptococcosis (52) and is highly recommended in combination with AMB for initial treatment of acute fungal meningitis and cryptococcosis (9, 50). Despite this clinical importance, the regulatory and resistance mechanisms for flucytosine in *C. neoformans* are poorly understood and have generally been assumed to be similar to those of *Saccharomyces cerevisiae* and *Candida albicans* (55). Flucytosine is transported into the cell by membrane-bound cytosine permease and converted to 5-fluorouracil by cytosine deaminase. Subsequently, 5-fluorouracil is converted to 5-fluoro-UMP by uracil phosphoribosyltransferase (UPRT), which is further metabolized to either

Received 8 September 2011 **Accepted** 28 October 2011
Published ahead of print 11 November 2011
Address correspondence to Yong-Sun Bahn, ysbahn@yonsei.ac.kr.
M.-H. Song and J.-W. Lee contributed equally to this article.
Supplemental material for this article may be found at http://ec.asm.org/.

doi:10.1128/EC.05236-11

5-fluoro-UTP or 5-fluoro-2′-deoxyuridylate, the last two of which inhibit RNA and DNA synthesis, respectively (52).

Here we found that a *C. neoformans* strain lacking the hybrid sensor kinase Tco1 or Tco2 exhibited differential susceptibility to flucytosine, suggesting that the two-component system may be involved in a flucytosine resistance mechanism. The cryptococcal two-component system, composed of hybrid sensor kinases (Tco1/2), phosphotransfer protein (Ypd1), and response regulators (Ssk1 and Skn7), activates the Ssk2-Pbs2-Hog1 mitogen-activated protein kinase (MAPK) module (6, 7, 33). Hog1 subsequently activates a plethora of downstream target genes which control a variety of cellular functions in *C. neoformans*, including stress response, sexual differentiation, ergosterol biosynthesis, and production of two major virulence factors, capsule and melanin (6, 29). Notably, perturbation of the two-component system and HOG pathway dramatically increases susceptibility to polyene drugs, such as AMB, mainly due to increased cellular ergosterol content (29). To identify and characterize the flucytosine-responsive genes in *C. neoformans* at the genome level, we performed a comparative transcriptome analysis of the wild-type (WT) strain and *tco1*Δ, *tco2*Δ, and *hog1*Δ mutants grown with or without flucytosine. Among 194 genes identified, we discovered a gene (CNAG_07464.2) that is predicted to encode a protein homologous to the yeast Mbp1 and Swi4 and therefore named it *MBS1* (Mbp1- and Swi4-like protein 1). In *S. cerevisiae*, Mbp1 is a DNA-binding protein that forms the MBF (MCB binding factor) complex with Swi6. During the cell cycle, MBF is involved in the G_1/S transition along with the SBF (Swi4/6 cell cycle box [SCB] binding factor) complex, which consists of Swi4 and Swi6. Mbp1 is homologous to Swi4, and double mutation of *MBP1* and *SWI4* causes lethality, indicating that Mbp1 and Swi4 play overlapping roles for the G_1/S transition in cell cycle progression (31). Mbp1 and Swi4 show limited but significant homology to fungal APSES proteins (19, 31, 48). The APSES transcription factors belong to the basic helix-loop-helix (bHLH) class of transcription factors, which is widely conserved in eukaryotic organisms, although the APSES domain itself is exclusively found in the fungal kingdom (19, 48). The APSES family of transcriptional regulatory proteins plays crucial roles in controlling morphological differentiation and virulence attributes in diverse fungal species (2, 20, 21, 36, 42, 43, 51, 54).

In this study, a variety of molecular and genetic analyses revealed that Mbs1 is indeed a flucytosine-responsive Mbp1/Swi4-like protein in the Tco2- and Hog1-related signaling pathways and plays pleiotropic roles in antifungal drug resistance by controlling ergosterol biosynthesis, oxidative and genotoxic stress response, and virulence of *C. neoformans*. Therefore, this study not only reports the first cryptococcal APSES-like protein but also may have identified a novel antifungal therapeutic method for treatment of cryptococcosis.

MATERIALS AND METHODS

Strains and growth media. The strains and primers used in this study are listed in Tables S1 and S2 in the supplemental material. *C. neoformans* strains were cultured in yeast extract-peptone-dextrose (YPD) medium unless indicated otherwise. Agar-based Dulbecco modified Eagle (DME) medium for capsule production and L-3,4-dihydroxyphenylalanine (L-DOPA) medium or Niger seed medium for melanin production were prepared as described previously (1, 5, 22, 26).

Antifungal drug and stress susceptibility tests. To assess stress response and antifungal drug susceptibility, cells grown overnight at 30°C in YPD medium were serially diluted (1 to 10^4 dilutions) with sterile H_2O. Then 3 to 4 μl of cell suspension of each strain was spotted onto solid YPD or yeast extract-peptone (YP) agar medium containing the indicated concentrations of flucytosine, amphotericin B, fluconazole, ketoconazole, itraconazole, or fludioxonil for antifungal drug susceptibility testing; NaCl or KCl for osmosensitivity test; hydrogen peroxide, diamide, or *tert*-butyl hydroperoxide for oxidative stress susceptibility test; hydroxyurea or methyl methanesulfonate for genotoxic stress susceptibility test; and cadmium sulfate for heavy metal stress test. Plates were observed after 2 to 4 days of incubation at 30°C and photographed.

Total RNA isolation and DNA microarray analysis. Total RNA for DNA was obtained by growing the WT H99 strain and *tco1*Δ (YSB355), *tco2*Δ (YSB281), and *hog1*Δ (YSB64) mutant strains in 50 ml YPD medium at 30°C for 16 h. Then 5 ml of the overnight culture was inoculated into 100 ml of fresh YPD medium and further incubated for 4 h at 30°C to an optical density at 600 nm (OD_{600}) of 1.0. The inoculated 100 ml YPD medium was divided into two 50-ml flasks, one with and one without 25 μg/ml flucytosine treatment, and both flasks were incubated for 90 min at 30°C. Then the culture was frozen in liquid nitrogen and lyophilized overnight. Three independent cultures for each strain were prepared for total RNA isolation as biological replicates. Total RNAs were isolated by the TRIzol reagent (Molecular Research Center) as described before (29). The concentration and purity of total RNA samples were measured by determination of the OD_{260} and gel electrophoresis. As control total RNAs for identifying flucytosine-responsive genes, all total RNAs prepared from WT and *tco1*Δ, *tco2*Δ, and *hog1*Δ mutant cells grown under the conditions described above were pooled as reference RNAs.

For DNA microarray analysis, we used a *C. neoformans* serotype D 70-mer microarray slide containing 7,936 probes (Duke University). The cDNA was synthesized by using AffinityScript reverse transcriptase (Stratagene), labeled by Cy5/Cy3 labeling agents (Amersham), hybridized to microarray slides, and then washed as described previously (29). Three independent DNA microarray analyses with three independent biological replicates were performed. Subsequently, hybridized chips were scanned with a GenePix 4000B scanner (Axon Instrument) and the signals were processed with the program GenePix Pro (version 4.0) and the GenePix array list (GAL) file (http://genome.wustl.edu/activity/ma/cneoformans). Microarray data analysis was performed as described previously (40). For hierarchical and statistical analysis, data transported from GenePix software were analyzed with Accuity software by employing Lowess normalization, reliable gene filtering (>95% filtering), hierarchical clustering, zero transformation, analysis of variance (ANOVA) ($P < 0.05$), and Microsoft Excel software (Microsoft).

Northern blot analysis and quantitative real-time reverse transcription-PCR. Quantitative real-time reverse transcription-PCR (qRT-PCR) for quantitatively measuring relative expression levels of *MBS1* and *ERG11* was performed with primers listed in Table S2 in the supplemental material and with cDNAs that were generated using the SuperScript II reverse transcriptase system with total RNAs used in DNA microarray analysis. Relative gene expression was calculated by the $2^{-\Delta\Delta CT}$ (where C_T is cycle threshold) method (35). *ACT1* was used for normalization of gene expression. Northern blot analysis for monitoring expression levels of *FCY1*, *FCY2*, *FCY4*, *FUR1*, and *MBS1* was performed as described previously (26).

Mutant and complemented strain construction. The *mbs1*Δ mutants were generated in the congenic *C. neoformans* serotype A *MAT*α (H99) and *MAT***a** (KN99**a**) strain background by overlap PCR by using H99 or KN99**a** genomic DNA and primers listed in Table S2 in the supplemental material as described previously (6, 17). Positive mutant strains were screened by using diagnostic PCR screening primers and further confirmed by Southern blot analysis with a genomic DNA digested with appropriate restriction enzymes, and each gene-specific probe was amplified by PCR with primers listed in Table S2 in the supplemental material (see also Fig. S2B in the supplemental material).

To verify mutant phenotypes, the *mbs1*Δ/*MBS1* complemented

strains were constructed by reintegrating the WT *MBS1* gene into the native *MBS1* locus as follows. First, the full-length *MBS1* gene, which contains 1,077 bp of the 5′ untranslated region (UTR), 2,301 bp of the *MBS1* open reading frame (ORF), and 400 bp of the 3′ UTR, was amplified by PCR with H99 genomic DNA as a template and primers B1958 and B1959 containing a NotI recognition site and directly cloned into the TOP vector (Enzynomics) to generate plasmid pCR-MBS1. After confirming the DNA sequence, the *MBS1* insert was subcloned into plasmid pJAF12 (NEO^r) to produce plasmid pNEOMBS1. For the targeted reintegration of the WT *MBS1* allele into its native locus, pNEOMBS1 was linearized by digestion with MfeI, of which the restriction site is uniquely present in the *MBS1* promoter region of the plasmid, and biolistically transformed into the *mbs1*Δ mutant (YSB488). Targeted reintegration of the *MBS1* gene into its native locus (YSB1195) was confirmed by diagnostic PCR with the primer pair of B1216, which binds upstream of the *MBS1* promoter region of pNEOMBS1, and B2303, which binds to the 4th exon of the *MBS1* coding sequence (see Fig. S2A and C in the supplemental material).

Cytosine uptake by fungal cells. Cytosine uptake in the WT H99 strain, along with the *tco1*Δ and *tco2*Δ mutants, was determined using [^{3}H]cytosine (specific activity, 20 Ci/mmol; Moravek Biochemicals). Cells were grown overnight in YPD medium at 30°C for 48 h to an OD_{600} of typically between 2.0 and 4.0. Cells were subsequently harvested by centrifugation (3,000 × *g*, 5 min) and washed twice with YNB complete medium (1.7 g yeast nitrogen base without amino acids or ammonium sulfate, 5 g ammonium sulfate per liter, pH 5.0) with or without glucose (for starvation) and without supplementation. Cells were resuspended at a cell density corresponding to an absorbance at 600 nm of 30 in YNB medium for 3 h for glucose starvation and then incubated in the presence of 50 nM [^{3}H]cytosine. Samples (100 μl) were removed at 1 h, 3 h, and 24 h and placed into stop solution (YNB medium plus 20 μM [3 mg/ml] fluconazole), filtered on glass fiber filters (pore size, 24 mm; GF/C; Whatman, Kent, United Kingdom) made wet beforehand with stop solution, and washed once with 5 ml of stop solution. Filters were transferred to 20-ml scintillation vials. Scintillation cocktail (Ecoscint XR; National Diagnostics, Atlanta, GA) was added (15 ml), and the vials were left at room temperature overnight before they were read. The radioactivity associated with the filter was measured with a liquid scintillation analyzer (Tri-Carb 2800 TR; Perkin Elmer, Waltham, MA) and normalized to cpm/1 × 10^8 cells. Samples were analyzed for [^{3}H]cytosine accumulation at designated time points.

Assays for melanin, capsule, and ergosterol production. Qualitative visualization and quantitative measurement of capsule and melanin production were performed as described previously (26, 28). Ergosterol extraction and calculation of ergosterol content were done following the method outlined by Ko et al. (29).

Virulence assay. All animal experiments were done at the University of Minnesota in strict accordance with good animal practice as defined by the National Institutes of Health Office of Laboratory Animal Welfare (OLAW) and the Association for the Assessment and Accreditation of Laboratory Animal Care (AAALAC). All experiments were reviewed and approved by the University of Minnesota Institutional Animal Care and Use Committee (IACUC) under protocol number 1010A91133. Overnight cultures of *C. neoformans* strain H99 and the *mbs1*Δ (YSB488) and *mbs1*Δ/*MBS1* (YSB1195) mutants were grown in YPD broth at 30°C. The resulting cultured yeast cells were pelleted and washed three times in sterile phosphate-buffered saline (PBS). For each strain, hemocytometer counts were utilized to adjust cell concentrations to 1 × 10^6 cells/ml. Groups of 10 6- to 8-week-old female A/J mice (Jackson Laboratory, Bar Harbor, ME) were anesthetized by intraperitoneal pentobarbital injection. Using a murine inhalation model, 5 × 10^4 cells in 0.05 ml PBS were instilled into the nares of anesthetized mice. The concentration of the initial inoculum was confirmed by plating serial dilutions on YPD agar and enumerating the CFU. Mice were monitored daily for signs of severe morbidity (weight loss, abnormal gait, extension of the cerebral portion of the cranium). Animals exhibiting these signs were sacrificed by CO_2 inhalation. Homogenized lung, spleen, and brain tissues from representative animals from each infection were plated onto YPD agar containing chloramphenicol (100 mg/ml) to determine the numbers of CFU and the extent of dissemination. Survival data were analyzed by the Analyze-It for Excel program. The Mann-Whitney U test was performed to analyze differences between survival curves, and *P* values of <0.05 were considered significant.

Tissue analysis. Groups of 3 mice were infected with 5 × 10^4 cells of the H99, *mbs1*Δ, or *mbs1*Δ/*MBS1* strain as described above. Infected mice were sacrificed at 21 days postinfection by CO_2 inhalation. The lungs and brain were harvested, fixed in 10% buffered formalin, paraffin embedded, sectioned, and stained with hematoxylin and eosin (H&E). Tissue sections were examined for cell size and morphology, as well as signs of host immune response, by microscopy.

Titan cell formation. Three mice per treatment were infected with 5 × 10^6 cells of the H99, *mbs1*Δ, or *mbs1*Δ/*MBS1* strain as described above. At 3 days postinfection, animals were sacrificed by CO_2 inhalation. Lungs were lavaged with 1.5 ml sterile PBS three times using a 20-gauge needle placed in the trachea. Cells in the lavage fluid were pelleted at 16,000 × *g* and subjected to a 30-min room temperature fixation in a 3.7% formaldehyde solution. Cells were subsequently washed once with PBS, resuspended in PBS, and analyzed for size and morphology by microscopy. A minimum of 300 cells per animal were analyzed to determine the extent of titan cell formation. One-way ANOVA was used to analyze differences in titan cell production. *P* values of less than 0.05 were considered significant.

Microarray data accession number. The whole microarray data generated by this study have been submitted to the Gene Expression Omnibus (GEO; http://www.ncbi.nlm.nih.gov/geo/) under accession no. GSE30154.

RESULTS

Role of hybrid sensor kinases Tco1 and Tco2 in flucytosine resistance of *C. neoformans*. To find synergistic cellular targets for combination therapy with flucytosine, we tested the flucytosine susceptibility of different two-component system and HOG signaling mutants in *C. neoformans*. Cells with Hog1 MAPK (*hog1*Δ), Pbs2 MAPKK (*pbs2*Δ), and Ssk2 MAPKKK (*ssk2*Δ) deletions were slightly more susceptible to flucytosine than the WT strain (Fig. 1A). Intriguingly, two major hybrid sensor kinases, Tco1 and Tco2, appeared to control flucytosine resistance in *C. neoformans* in opposing manners (Fig. 1A). Mutation of *TCO1*, which encodes a HAMP repeat-containing hybrid sensor kinase, enhanced flucytosine susceptibility, whereas mutation of *TCO2*, which encodes a double-hybrid sensor kinase, conferred flucytosine resistance (Fig. 1A). In contrast, other hybrid sensor kinase mutants, including *tco3*Δ, *tco4*Δ, *tco5*Δ, and *tco7*Δ mutants, showed WT levels of susceptibility to flucytosine (Fig. 1A). These results indicate that the two-component phosphorelay system may be involved in flucytosine resistance in *C. neoformans*.

Involvement of the two-component phosphorelay system in flucytosine resistance has not been reported in other fungi. Therefore, we investigated how the phosphorelay system and hybrid sensor kinase mutants show differential susceptibility against flucytosine in *C. neoformans*. The general mode of action for developing flucytosine resistance has been well characterized in other fungi (52) (see Fig. S1 in the supplemental material). *C. neoformans* contains homologs of cytosine permease genes (CNAG_01681.2, CNAG_04982.2, and CNAG_04276.2; we named them *FCY2*, *FCY3*, and *FCY4*, respectively) and cytosine deaminase genes (CNAG_00613.2, which we named *FCY1*), and the UPRT gene (CNAG_02337.2, which we named *FUR1*) (see Fig. S1 in the supplemental material). Therefore, the flucytosine

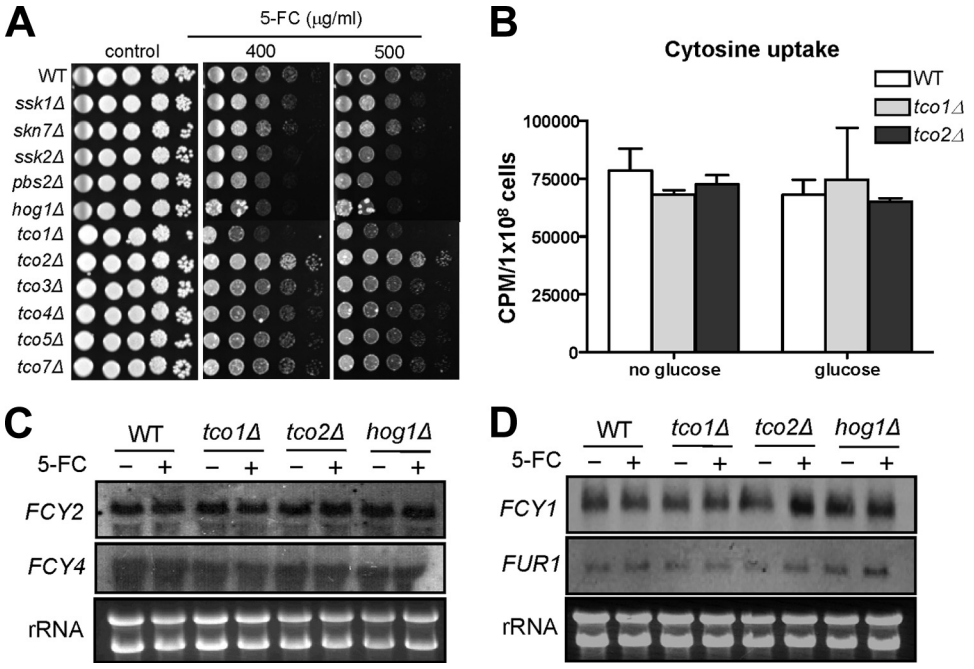

FIG 1 Role of the two-component system and the HOG pathway in flucytosine susceptibility of *C. neoformans*. (A) Each *C. neoformans* strain (WT [H99], *hog1*Δ [YSB64], *pbs2*Δ [YSB123], *ssk2*Δ [YSB264], *ssk1*Δ [YSB261], *skn7*Δ [YSB349], *tco1*Δ [YSB278], *tco2*Δ [YSB281], *tco3*Δ [YSB284], *tco4*Δ [YSB417], *tco5*Δ [YSB286], and *tco7*Δ [YSB348]) was grown overnight at 30°C in liquid YPD medium, 10-fold serially diluted (1 to 10^4 dilutions), and spotted (3 μl of dilution) on YPD agar containing the indicated concentrations of flucytosine. Cells were incubated at 30°C for 72 h and photographed. (B) Cytosine uptake test. Uptake of radiolabeled cytosine ([^{3}H]cytosine) into the WT strain and *tco1*Δ and *tco2*Δ mutants was quantitatively measured as described in Materials and Methods. (C and D) Northern blot analysis for monitoring expression levels of genes (*FCY1* [cytosine deaminase, CNAG_00613.2], *FCY2* [cytosine permease, CNAG_01681.2], *FCY4* [cytosine permeases, CNAG_04276.2], and *FUR1* [uracil phosphoribosyltransferase, CNAG_02337.2]) involved in flucytosine uptake and metabolism. Total RNA isolated from the WT strain and *tco1*Δ, *tco2*Δ, and *hog1*Δ mutants grown at 30°C for 90 min in YPD medium with or without 25 μg/ml of flucytosine (5-FC) was used for Northern blot analysis by using the gene-specific probes listed in Table S2 in the supplemental material.

resistance observed in the two-component system mutants could be the result of altered expression of genes encoding cytosine permease, cytosine deaminase, or UPRT (11, 52).

To compare flucytosine uptake levels between the WT strain and *tco1*Δ and *tco2*Δ mutants, we measured intracellular accumulation of radiolabeled cytosine in the WT strain and *tco1*Δ and *tco2*Δ mutants based on the fact that flucytosine is transferred into the cell and metabolized similarly to exogenously added cytosine. Lack of Tco1 and Tco2 did not affect cellular uptake of cytosine under either glucose-rich or glucose-starved conditions (Fig. 1B). Supporting this finding, expression levels of the cytosine permease genes *FCY2* and *FCY4* in the *tco1*Δ or *tco2*Δ mutant were found to be similar to those in the WT strain before and after flucytosine treatment (Fig. 1C). Transcript abundance of *FCY3* was too low to be detected in the WT strain and *tco1*Δ and *tco2*Δ mutants (data not shown). Expression levels of *FCY1* were also not altered in the WT strains and *tco1*Δ mutant in response to flucytosine. However, *FCY1* expression was induced in the *tco2*Δ mutant upon flucytosine treatment (Fig. 1D). *FUR1* expression was not significantly altered in the WT strain and *tco1*Δ and *tco2*Δ mutants upon flucytosine treatment (Fig. 1D). Interestingly, basal expression levels of *FUR1* and *FCY1* appeared to be higher in the *hog1*Δ mutant than WT (Fig. 1D). Nevertheless, these expression patterns of genes involved in the salvage pathway of cytosine metabolism did not appear to be correlated with the differential flucytosine susceptibility patterns observed in the *tco1*Δ and *tco2*Δ mutants. Hence, we concluded that the differential flucytosine resistance observed in *tco1*Δ and *tco2*Δ mutants may result from aberrant regulation of a signaling or metabolic pathway(s) other than the salvage pathway of cytosine metabolism.

Comparative transcriptome analysis of the *tco1*Δ, *tco2*Δ, and *hog1*Δ mutants in response to flucytosine treatment. To address how Tco1, Tco2, and Hog1 differentially regulate flucytosine resistance and to discover genes that are regulated by flucytosine in *C. neoformans*, we performed comparative transcriptome analysis of the WT strain and *tco1*Δ, *tco2*Δ, and *hog1*Δ mutants with or without flucytosine treatment. Previously, Zhang and coworkers performed a similar transcriptome analysis to find flucytosine-responsive genes by using DNA microarray analysis with total RNA isolated from *Saccharomyces cerevisiae* grown in YPD medium containing 25 μg/ml flucytosine for 90 min (57). We found that the concentration of 25 μg/ml was also close to a sublethal concentration of flucytosine without affecting cell viability of *C. neoformans* at a 90-min incubation time (data not shown). Therefore, we decided to use the same concentration and incubation time for flucytosine treatment for total RNA isolation from *C. neoformans* strains, which allowed us to compare transcriptome profiles for flucytosine-responsive genes between *C. neoformans* and *S. cerevisiae*. The whole microarray data set is presented in Table S3 in the supplemental material.

Based on our transcriptome analysis, a total of 177 *C. neoformans* genes were up- or downregulated more than 2-fold in response to flucytosine (Fig. 2A to C; see Table S4 in the supplemental material). Among these, 118 genes encode proteins that do not

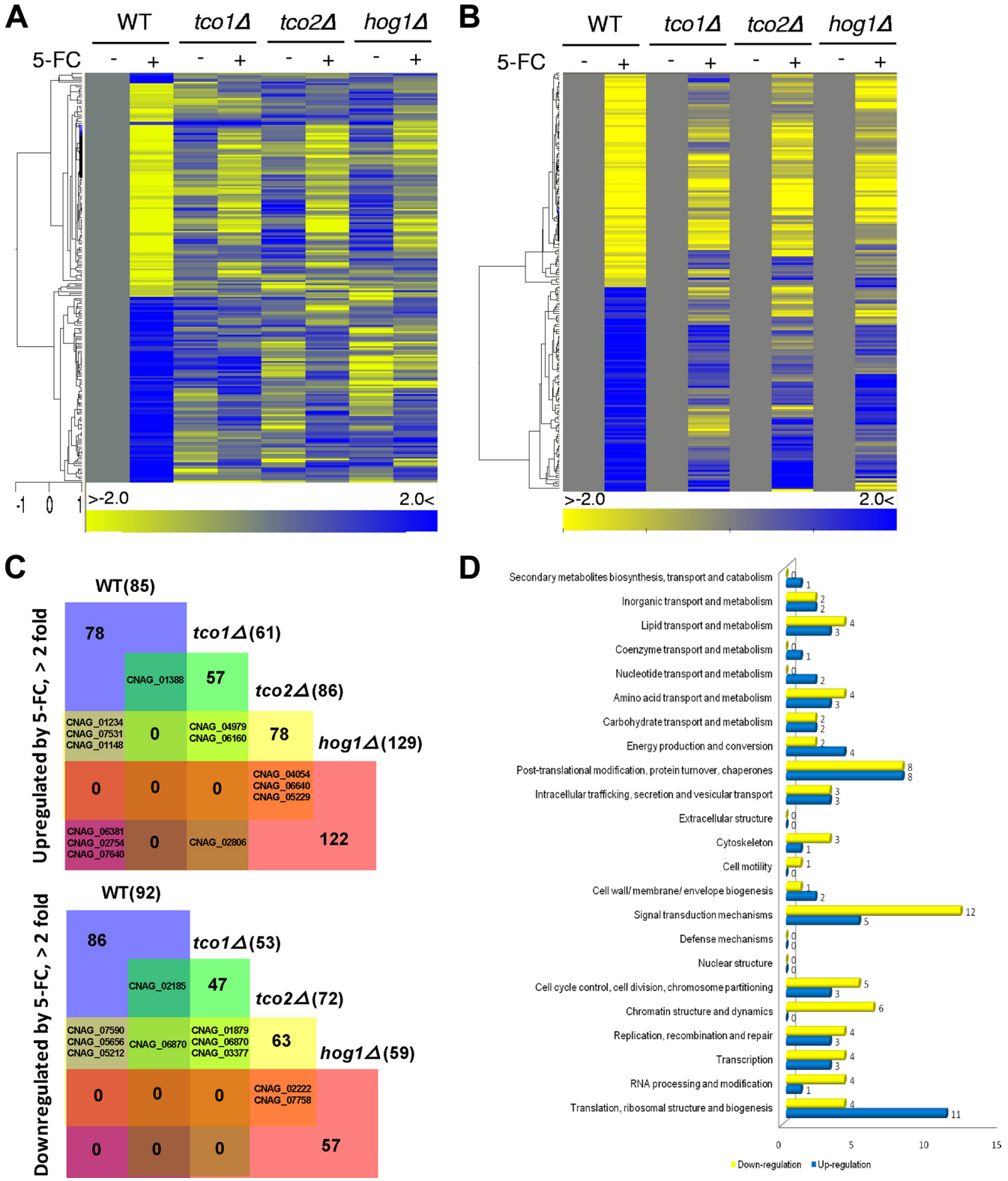

FIG 2 Transcriptome analysis of flucytosine-responsive genes in *C. neoformans*. (A and B) Hierarchical clustering of the expression profiles of 177 flucytosine stress-specific response genes in the WT strain and *tco1*Δ, *tco2*Δ, and *hog1*Δ mutants is illustrated ($P < 0.05$, > 2-fold). The change (fold) is illustrated by color (see the bar scale). (A) All fold changes in each mutant with or without exposure to flucytosine were determined by normalizing (zero transformation) expression levels of each gene to those in the WT strain without exposure to flucytosine (see Table S4 in the supplemental material). (B) All fold changes in response to flucytosine were determined individually in each mutant by normalizing (zero transformation) expression levels of each gene with exposure to flucytosine to those without exposure to flucytosine (see Tables S5 and S6 in the supplemental material). (C) Venn diagram showing flucytosine-responsive genes in the WT strain and *tco1*Δ, *tco2*Δ, and *hog1*Δ mutants (see Table S7 in the supplemental material). (D) Functional KOG (eukaryotic orthologous group) categories of genes differentially regulated by flucytosine treatment in the WT strain.

show significant homology to any known proteins (see Table S5 in the supplemental material). The remaining 59 genes had orthologs in *S. cerevisiae* or other fungi (Table 1; see Table S6 in the supplemental material). Strikingly, however, none of the 59 genes overlap with those of flucytosine-responsive genes in *S. cerevisiae* (57). These data indicate that *C. neoformans* may employ a unique set of genes to counteract flucytosine. Among flucytosine-responsive genes with known or predicted functions, major functional categories include signal transduction mechanisms (17 genes), posttranslational modification and protein turnover (16 genes), translation, ribosomal structure, and biogenesis (15 genes), and cell cycle control, cell division, and chromosome partitioning (8 genes) (Fig. 2D). These findings indicate that cellular adaptation against flucytosine requires active modulation of various signaling and metabolic pathways, which may include the Tco1/2-dependent two-component system. Flucytosine incorporation into DNA and RNA molecules may lead to production and accumulation of truncated, nonfunctional, toxic proteins, which explains why a number of genes that are involved in translation and posttranslational modification or their quality control were found to be regulated by flucytosine. Genes that are involved in cell cycle control appear to be also required for cellular growth control in the presence of a toxic nucleoside analogue. Notably, a significant portion of the flucytosine-responsive genes in *C. neoformans* was found to be differentially regulated in the *tco1*Δ, *tco2*Δ, or *hog1*Δ mutants compared to the WT strain (Fig. 2A to C; see Table S7 in the supplemental material), indicating that the two-component system and HOG pathways are major elements for flucytosine resistance in *C. neoformans*.

Discovery of a flucytosine-responsive Mbp1/Swi4-like protein, Mbs1, in *C. neoformans*. Among the flucytosine-responsive and two-component system-dependent genes, we focused on a putative transcription factor which could potentially regulate expression of various flucytosine-defense genes in *C. neoformans*. CNAG_07464.2 was predicted to encode a protein that is homologous to Mbp1 and Swi4 in *S. cerevisiae*. Hence, we named this gene *MBS1* (Mbp1- and Swi4-like protein 1). Mbp1 and Swi4 show limited but significant sequence homology to a family of APSES transcription factors which are widely conserved in the fungal kingdom but not in other eukaryotic kingdoms or prokaryotes (48). Protein domain analysis by the Pfam database (http://pfam.sanger.ac.uk/) revealed that Mbs1 contains a KilA-N DNA-binding domain at the amino terminus which is found in APSES proteins and Mbp1/Swi4-like proteins (see Fig. S2 in the supplemental material). In addition, the ankyrin repeat domain, which is known to mediate protein-protein interaction, is also observed in CNAG_07464.2, similar to yeast Mbp1 (see Fig. S2 in the supplemental material). Multiple-sequence alignment revealed that the 97 amino acids of Mbs1 (Y to Y) showed limited but significant homology to similar domains of other fungal APSES proteins, whereas they are highly homologous to the DNA-binding domains of Mbp1 and Swi4 (Fig. 3A).

We first confirmed whether *MBS1* expression is controlled by flucytosine via the two-component system. qRT-PCR clearly showed that *MBS1* is induced in response to flucytosine in the WT and *tco1*Δ strains (Fig. 3B). In the *tco2*Δ mutant, however, basal expression levels of *MBS1* induction were slightly increased, but the *MBS1* expression was not further induced in response to flucytosine (Fig. 3B). Interestingly, both basal and induced levels of *MBS1* were higher in the *hog1*Δ mutant than WT (Fig. 3B). Northern blot analysis confirmed these results (data not shown). These data suggest that Tco2 and Hog1 play a role in controlling *MBS1* expression.

To address whether Mbs1 is indeed required for flucytosine resistance of *C. neoformans*, we generated two independent *mbs1*Δ mutants and confirmed that the two independent *mbs1*Δ mutants are phenotypically identical (data not shown). The *mbs1*Δ mutants and *mbs1*Δ/*MBS1* complemented strains grew as well as WT in either solid or liquid YPD medium at 30°C and 37°C, which is a host physiological temperature (see Fig. S4 in the supplemental material). However, the *mbs1*Δ mutant exhibited a minor defect in growth at a higher temperature (39°C) on solid YPD medium (see Fig. S4A in the supplemental material), although this minor growth defect at 39°C was not detectable in liquid YPD medium (see Fig. S4B in the supplemental material), implying the potential involvement of Mbs1 in thermotolerance. As expected from expression analysis of *MBS1*, the *mbs1*Δ mutants exhibited much greater susceptibility to flucytosine than WT and its complemented strain (Fig. 3C). Taken together, these results demonstrate that Mbs1 is a flucytosine-responsive APSES-like protein that controls the flucytosine resistance of *C. neoformans*.

Mbs1 affects ergosterol biosynthesis and thereby controls polyene and azole drug susceptibility of *C. neoformans*. Because *MBS1* expression appeared to be regulated by Tco2 and Hog1, we examined other Tco2- and Hog1-dependent phenotypes in *C. neoformans*. Our prior study showed that the *hog1*Δ, *pbs2*Δ, *ssk2*Δ, and *ssk1*Δ mutants all showed increased susceptibility to amphotericin B (AMB), whereas they were resistant to azole antifungal drugs, such as fluconazole and ketoconazole (29). In contrast, the *tco2*Δ mutant exhibited increased susceptibility to AMB but displayed WT levels of resistance to azole drugs (29). The *mbs1*Δ mutant exhibited greater susceptibility to AMB than WT, albeit to a lesser extent than the *hog1*Δ mutant, but increased resistance to ketoconazole and fluconazole compared to WT at levels almost equivalent to those for the *hog1*Δ mutant (Fig. 4A).

The finding that the *mbs1*Δ mutant exhibited greater susceptibility to AMB and resistance to azole drugs suggested that Mbs1 could be a transcription factor affecting ergosterol biosynthesis in *C. neoformans* by controlling expression of *ERG11*, which encodes lanosterol 14α-demethylase, a target for the azole drugs. To address this question, we monitored *ERG11* expression in the *mbs1*Δ mutant compared to WT by qRT-PCR. Basal transcript levels of *ERG11* were much higher in the *mbs1*Δ mutant, albeit to a lesser extent than the *hog1*Δ mutant, than in WT (Fig. 4B). Furthermore, actual cellular ergosterol contents measured in the *mbs1*Δ mutant were higher than those measured in WT but lower than those measured in the *hog1*Δ mutant, which was in agreement with *ERG11* expression patterns (Fig. 4B and C). These results suggested that differential susceptibility to polyene and azole drugs in the *mbs1*Δ mutant is caused by altered amounts of ergosterol in the membrane (the polyene target) and Erg11 (the azole target) produced by cells.

Mbs1 is involved in maintenance of membrane stability and osmotic stress response. Changes in sterol content may affect membrane structure without having a direct influence on the regulation of membrane-lipid metabolism (23, 41). Therefore, we speculated that an increased ergosterol content may perturb normal cell membrane stability, as the *hog1*Δ mutant had increased ergosterol content and was hypersusceptible to a membrane detergent, such as SDS. Indeed, the *mbs1*Δ mutant exhibited hyper-

TABLE 1 Selected list of Tco1/2-dependent flucytosine-responsive genes

H99 identifier (CNAG no.)	*S. cerevisiae* identifier[a]	Fold change in expression				Functional description
		WT[b]	*tco1*Δ[c]	*tco2*Δ[d]	*hog1*Δ[e]	
06980	*STE11*	−1.593	1.528	−0.262	−1.592	Signal-transducing MEK kinase
01103	*PRP11*	−3.242	−0.635	−1.181	−2.135	Subunit of the SF3a splicing factor complex, required for spliceosome assembly
04521	*AIF1*	−1.676	0	0.309	−0.54	Mitochondrial cell death effectors
01412	*PAH1*	−1.211	−0.104	−0.243	−0.202	Mg^{2+}-dependent phosphatidate (PA) phosphatase
04604	*WRS1*	−1.331	−0.288	−0.589	−0.184	Cytoplasmic tryptophanyl-tRNA synthetase, aminoacylates tryptophanyl-tRNA
00689	*ALG1*	−2.168	−0.9	−1.238	−0.376	Mannosyltransferase
04451	*POP1*	−1.506	0.603	−1.109	−0.04	Subunit of both RNase MRP, which cleaves pre-rRNA, and nuclear RNase P
07590	*VMA5*	−1.694	0.184	−1.077	−0.162	Subunit C of the eight-subunit V1 peripheral membrane domain
04636	*MCA1*	−1.742	−0.151	−1.471	−0.47	Putative cysteine protease similar to mammalian caspases
07529	*ILV1*	−1.411	−0.997	−0.413	−1.133	Threonine deaminase, catalyzes the first step in isoleucine biosynthesis
03789	*MRT4*	−1.784	−0.377	−1.805	−0.895	Protein involved in mRNA turnover and ribosome assembly, localizes to the nucleolus
02940	*VNX1*	−3.929	−0.667	−2.344	−2.183	Low-affinity vacuolar membrane-localized monovalent cation/H^+ antiporter
02812	*ARG3*	−1.17	−0.054	−0.859	−0.695	Ornithine carbamoyltransferase (carbamoylphosphate:L-ornithine carbamoyltransferase)
01626	*ADA2*	−1.777	−1.581	−1.5	−0.063	Transcription coactivator
04902	*HRD3*	−1.329	−1.148	−0.775	−0.183	Resident protein of the endoplasmic reticulum
05898	*MET8*	−2.684	−2.341	−0.509	0.847	Bifunctional dehydrogenase and ferrochelatase
01885	*PAP2*	−1.381	0.23	0.744	−0.464	Catalytic subunit of TRAMP (Trf4/Pap2p-Mtr4p-Air1p/2p)
02233	*MEC1*	−1.199	0.415	0.442	0.31	Genome integrity checkpoint protein
02020	*SWC4*	−1.702	−0.787	0.932	−0.244	Component of the Swr1p complex
01175	*GOT1*	−1.112	1.642	1.824	1.635	Present in early Golgi cisternae
07464	*MBP1*	1.805	−0.428	−0.466	−0.502	Transcription factor involved in regulation of cell cycle progression from G_1 to S phase
03127	*RPS23B*	1.368	0.551	−0.999	0.614	Ribosomal protein 28 (rp28) of the small (40S) ribosomal subunit
02288	*SFC1*	2.147	−0.963	0.451	−0.952	Mitochondrial succinate-fumarate transporter
06223	*SIZ1*	2.274	0.911	−0.309	0.848	SUMO/Smt3 ligase that promotes the attachment of sumo (Smt3p)
06828	*AVT3*	1.86	0.752	−0.556	0.174	Vacuolar transporter
03565	*PMA1*	3.328	1.225	0.146	1.518	Plasma membrane H^+-ATPase, pumps protons out of the cell
03291	*GRH1*	2.6242	0.376	−0.042	1.274	Acetylated, *cis*-Golgi apparatus-localized protein
01592	*STE14*	4.076	0.596	0.472	−0.082	Farnesyl cysteine-carboxyl methyltransferase
00389	*IBA57*	1.368	0.653	0.296	0.268	Mitochondrial matrix protein
00640	*RPS4A*	2.057	0.723	0.232	0.198	Protein component of the small (40S) ribosomal subunit
01170	*RPS17A*	1.97	1.188	0.446	−0.021	Ribosomal protein 51 (rp51) of the small (40S) ribosomal subunit
05671	*OXR1*	1.309	0.848	0.07	1.729	Required for normal levels of resistance to oxidative damage
02884	*PSF2*	1.461	−0.084	0.473	0.968	Subunit of the GINS complex (Sld5p, Psf1p, Psf2p, Psf3p)
00703	*RPL31A*	2.008	−0.14	0.765	1.303	Protein component of the large (60S) ribosomal subunit
05862	*RAD10*	2.384	0.349	0.978	1.827	Single-stranded DNA endonuclease (with Rad1p)
02294	*ADE2*	2.799	−0.083	0.707	1.184	Phosphoribosylaminoimidazole carboxylase
02309	*FPR2*	1.305	−0.122	−0.649	1.124	Membrane-bound peptidyl-prolyl *cis-trans* isomerase (PPIase)
05248	*APL2*	1.745	0.01	−0.082	1.353	Beta-adaptin, large subunit of the clathrin-associated protein (AP-1) complex
03078	*NPP1*	2.013	−0.629	−0.525	1.165	Nucleotide pyrophosphatase/phosphodiesterase family member
05134	*CAR2*	1.095	−0.908	0.817	1.323	L-Ornithine transaminase (OTAse)
06447	*RPL17A*	1.624	−1.206	0.536	0.284	Protein component of the large (60S) ribosomal subunit
03352	*FRA2*	2.823	−3.459	1.273	0.939	Protein involved in negative regulation of transcription of iron regulon
06510	*APC2*	1.005	−0.11	1.361	0.501	Subunit of the anaphase-promoting complex/cyclosome (APC/C)
07531	*SNO1*	1.321	−0.109	1.14	−0.245	Protein of unconfirmed function, involved in pyridoxine metabolism
01976	*RPL23B*	2.358	0.336	1.258	0.205	Protein component of the large (60S) ribosomal subunit
03150	*FLX1*	1.842	0.459	1.245	0.411	Protein required for transport of flavin adenine dinucleotide (FAD)
00672	*RPS11A*	2.736	0.921	2.743	1.379	Protein component of the small (40S) ribosomal subunit
02754	*RPS12*	1.704	0.302	2.128	1.423	Protein component of the small (40S) ribosomal subunit

[a] *S. cerevisiae* identifier, the name of the *S. cerevisiae* gene orthologous to the corresponding *C. neoformans* gene.

[b] $\text{Log}_2[(\text{WT} + 5\text{FC})/(\text{WT} - 5\text{FC})]$, where (WT + 5FC) and (WT − 5FC) indicate expression levels of each gene in the wild-type strain with or without flucytosine (5FC) treatment, respectively.

[c] $\text{Log}_2[(\textit{tco1}\Delta + 5\text{FC})/(\textit{tco1}\Delta - 5\text{FC})]$, where (*tco1*Δ + 5FC) and (*tco1*Δ − 5FC) indicate expression levels of each gene in the *tco1*Δ mutant with or without flucytosine (5FC) treatment, respectively.

[d] $\text{Log}_2[(\textit{tco2}\Delta + 5\text{FC})/(\textit{tco2}\Delta - 5\text{FC})]$, where (*tco2*Δ + 5FC) and (*tco2*Δ − 5FC) indicate expression levels of each gene in the *tco2*Δ mutant with or without flucytosine (5FC) treatment, respectively.

[e] $\text{Log}_2[(\textit{hog1}\Delta + 5\text{FC})/(\textit{hog1}\Delta - 5\text{FC})]$, where (*hog1*Δ + 5FC) and (*hog1*Δ − 5FC) indicate expression levels of each gene in the *hog1*Δ mutant with or without flucytosine (5FC) treatment, respectively.

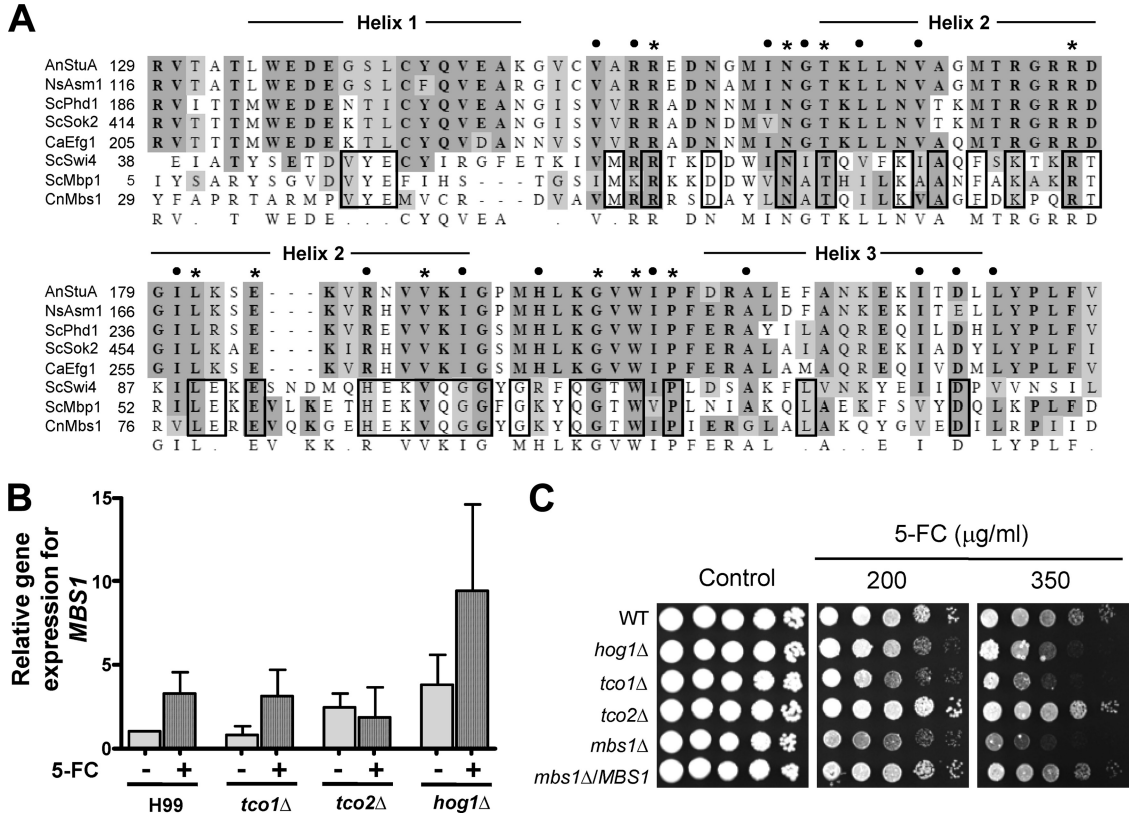

FIG 3 Identification, expression analysis, and functional characterization of *MBS1* in flucytosine susceptibility of *C. neoformans*. (A) Multiple-sequence alignment of the APSES-like DNA-binding domain of Mbs1 with similar domains of other APSES and Mbp1/Swi4 proteins. Each abbreviation indicates the following: AnStuA, *Aspergillus nidulans* StuA; NsAsm1, *Neurospora crassa* Asm1; ScPhd1 and ScSok2, *Saccharomyces cerevisiae* Phd1 and Sok2, respectively; CaEfg1, *Candida albicans* Efg1; ScSwi4 and ScMbp1, *S. cerevisiae* Swi4 and Mbp1, respectively; CnMbs1, *Cryptococcus neoformans* Mbs1. Residues in dark shades are identical, and homologous residues are included in light shades. Asterisks and closed circles indicate identical and similar residues, respectively, between APSES and APSES-like proteins. Identical residues between ScMbp1/Swi4 and CnMbs1 are marked with a solid-line box. (B) qRT-PCR for monitoring *MBS1* expression patterns in the WT strain (H99) and *tco1*Δ, *tco2*Δ, and *hog1*Δ mutants during flucytosine (5-FC) treatment. Total RNA isolated from each strain grown at 30°C for the indicated incubation time (90 min) in YPD medium with or without 25 μg/ml of flucytosine was used. Data were normalized by using *ACT1* as a control, and relative gene expression indicates *MBS1* expression of each strain compared to that of WT at zero time point. (C) Flucytosine susceptibility test. Each *C. neoformans* strain (the WT [H99], *hog1*Δ [YSB64], *tco1*Δ [YSB278], *tco2*Δ [YSB281], *mbs1*Δ [YSB 488], and *mbs1*Δ/*MBS1* [YSB1195] strains) was grown overnight at 30°C in liquid YPD medium, 10-fold serially diluted (1 to 10^4 dilutions), and spotted (3 μl of dilution) on YPD agar containing the indicated concentrations of flucytosine.

susceptibility to SDS, similar to the *hog1*Δ mutant (Fig. 5A). We addressed whether defective membrane stability also affected resistance to osmotic stress. Similar to the *hog1*Δ mutant, the *mbs1*Δ mutant was more susceptible to high concentrations of NaCl (data not shown) and KCl than WT (Fig. 5B). In conclusion, Mbs1 modulates cell membrane stability and resistance to the osmotic stress response.

Mbs1 is required for genotoxic and oxidative stress responses. In *S. cerevisiae*, Mbp1 and Swi4 play redundant roles in cell cycle regulation (8, 25, 31). Furthermore, our prior study demonstrated that Hog1 is also involved in defense against DNA-damaging agents (29). Therefore, we addressed whether Mbs1 controls cellular responses against genotoxic stresses, which may confer DNA damage and subsequent cell cycle arrest. We tested cellular susceptibility to two DNA-damaging agents, hydroxyurea (HU) and methyl methanesulfonate (MMS). HU is a ribonucleotide reductase inhibitor which blocks DNA synthesis and hinders the deoxynucleoside triphosphate pool expansion during G_1-to-S-phase transition (30). MMS is a DNA-alkylating agent which causes DNA fragmentation by inducing DNA double-strand breaks (38). The *mbs1*Δ mutant exhibited hypersusceptibility to HU, but not to MMS (data not shown), which was very similar to results for the *hog1*Δ mutant (Fig. 6A). Interestingly, however, the *mbs1*Δ mutant displayed extreme resistance to thiabendazole (TBZ), a microtubule-destabilizing drug, whereas both the *tco1*Δ and *tco2*Δ mutants but not the *hog1*Δ mutant exhibited minor TBZ resistance (Fig. 6A). Mutations perturbing centromere or kinetochore function are often TBZ susceptible.

In oxidative stress response, the *mbs1*Δ mutant exhibited phenotypes similar to those of the *hog1*Δ and *tco2*Δ mutants. We tested cellular susceptibility to hydrogen peroxide (H_2O_2) and diamide. H_2O_2 is one of the reactive oxygen species which can be endogenously generated during oxygen-consuming metabolism and induces protein thiol modification and radical formation. In contrast, diamide is an exogenous oxidant which is more specific toward thiol groups with glutathione but does not induce radical formation. Cellular responses to diamide and H_2O_2 are known to be different (see the review in reference 37). Similar to the *hog1*Δ and *tco2*Δ mutants, the *mbs1*Δ mutant displayed increased susceptibility and resistance to H_2O_2 and diamide, respectively (Fig.

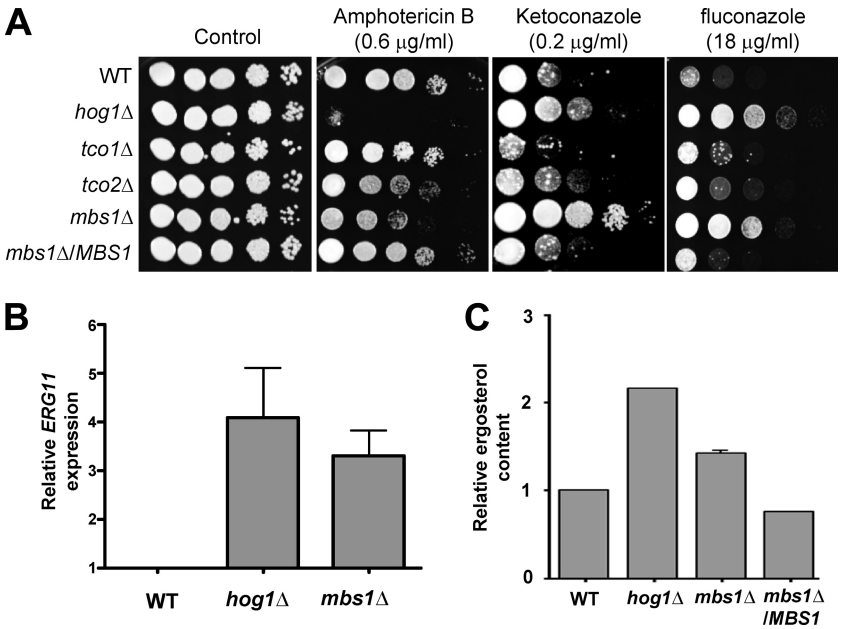

FIG 4 Role of Mbs1 in antifungal drug susceptibility and ergosterol biosynthesis. (A) Each *C. neoformans* strain described in Fig. 3B was grown overnight at 30°C in liquid YPD medium, 10-fold serially diluted (1 to 10^4 dilutions), and spotted (3 μl of dilution) on YPD agar containing the indicated concentrations of amphotericin B, ketoconazole, and fluconazole. (B) Quantitative RT-PCR showing transcript levels of *ERG11* in the WT strain and *hog1*Δ and *mbs1*Δ mutants. For qRT-PCR, *MBS1* expression data obtained from three independent biological replicates with three technical replicates were normalized by using *ACT1* as a control. Relative gene expression indicates *ERG11* expression levels normalized to those of the WT strain. (C) Cellular ergosterol content was measured as described in Materials and Methods. The graph demonstrates relative increase in ergosterol content compared to WT. Each bar demonstrates the average from four independent experiments, and error bars indicate the standard deviation.

6B). In contrast, the *mbs1*Δ mutant did not exhibit any increased susceptibility or resistance to fludioxonil (an inducer of intracellular glycerol accumulation), the heavy metal $CdSO_4$, or *tert*-butyl hydroperoxide, unlike the *hog1*Δ mutant (see Fig. S5 in the supplemental material). Taken together, these results suggested that Mbs1 is required for genotoxic stress response by potentially controlling cell cycle regulation and oxidative stress response.

Mbs1 modulates pathogenicity and the host immune response to infection. Next we measured the ability of the *mbs1*Δ mutant to produce virulence factors of *C. neoformans* because these attributes are also controlled by the two-component system and the HOG pathway. At physiological temperature (37°C), the *mbs1*Δ mutant produced much lower levels of melanin than WT,

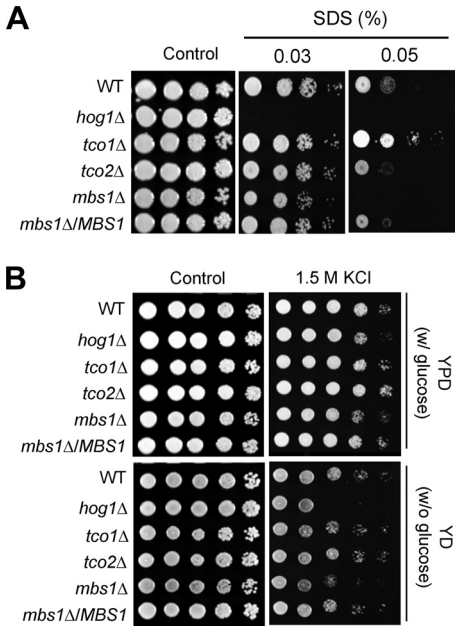

FIG 5 Role of Mbs1 in cell membrane integrity and osmotic stress response. Each *C. neoformans* strain described in Fig. 3B was grown overnight at 30°C in liquid YPD medium, 10-fold serially diluted, and spotted (3 μl of dilution) on YPD agar containing the indicated concentrations of SDS (A) or YP agar containing the indicated concentration of KCl (B).

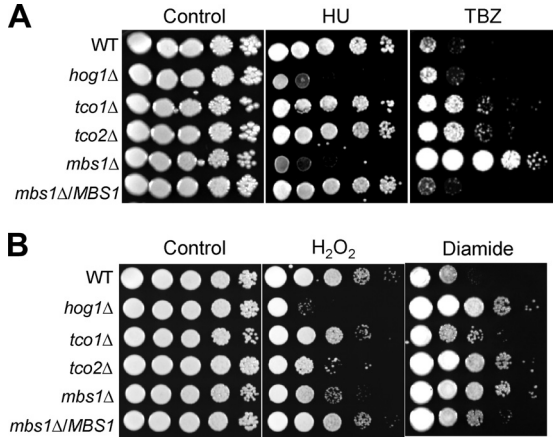

FIG 6 Role of Mbs1 in genotoxic and oxidative stress response. Each *C. neoformans* strain described in Fig. 3B was grown overnight at 30°C in liquid YPD medium, 10-fold serially diluted (1 to 10^4 dilutions), and spotted (3 μl of dilution) on YPD agar containing the indicated concentrations of HU (70 mM) or TBZ (11 μg/ml) for genotoxic stress susceptibility test (A) and H_2O_2 (2.5 mM) or diamide (3 mM) for oxidative stress susceptibility test (B).

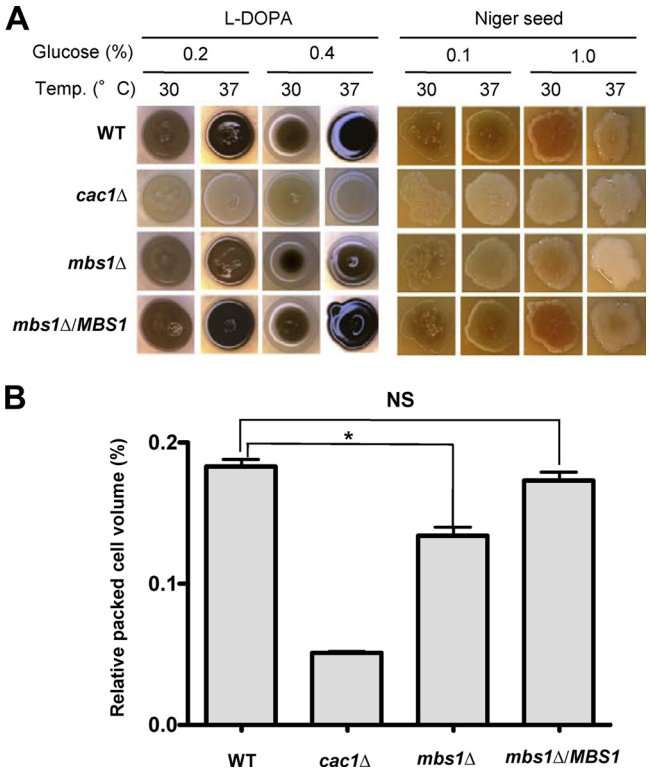

FIG 7 Mbs1 is involved in production of melanin and capsule. (A) For melanin assay, the WT (H99), *cac1*Δ (YSB42), *mbs1*Δ (YSB488), and *mbs1*Δ/*MBS1* (YSB1195) strains were spotted onto agar-based L-DOPA and Niger seed media containing the indicated concentration of glucose, grown at either 30°C or 37°C for 5 to 7 days, and photographed. (B) Capsule synthesis levels of *C. neoformans* strains (WT [H99], *cac1*Δ [YSB42], *mbs1*Δ [YSB488], and *mbs1*Δ/*MBS1* [YSB1195] strains) were quantitatively measured by using hematocrit, as described in Materials and Methods. The relative capsule volume of the cells was measured by calculating the ratio of the length of packed cell volume phase/length of total volume phase. Two independent experiments with triplicates were performed. Statistical analysis was performed by using the Bonferroni multiple-comparison test. NS, not significant; ∗, $P < 0.001$.

although the melanin synthesis defect of the *mbs1*Δ mutant was not as pronounced as that of the *cac1*Δ mutant, which is defective in cyclic AMP signaling (Fig. 7A). Similarly, the *mbs1*Δ mutant also exhibited a minor defect in capsule production compared to WT (Fig. 7B).

The role of Mbs1 in virulence factor production of *C. neoformans* prompted us to investigate whether Mbs1 is required for the pathogenicity of *C. neoformans*. The *mbs1*Δ mutant exhibited reduced virulence compared to WT in a murine survival model of systemic cryptococcosis (Fig. 8A). While mice infected with the WT strain became moribund 18 to 24 days postinfection, mice infected with the *mbs1*Δ mutant did not show illness until 26 days postinfection. In contrast to WT infections, animals infected with the *mbs1*Δ mutant strain did not develop signs of neurological involvement. On the basis of physical signs of weight loss coupled with labored breathing, mice infected with the *mbs1*Δ mutant strain appear to have succumbed to the pulmonary infection. In contrast, the *mbs1*Δ/*MBS1* complemented strains exhibited WT levels of virulence. When fungal burden was measured in moribund animals, the lungs, spleen, and brain from mice infected with the *mbs1*Δ mutant showed reduced fungal burden compared to the WT and *mbs1*Δ/*MBS1* complemented strains (Fig. 8B and data not shown).

During host infection, a subpopulation of *C. neoformans* undergoes cell size enlargement (up to 100 μm), which is particularly stimulated by coinfection with opposite-mating-type cells. The titan cells are uninucleate and polyploid and exhibit reduced phagocytosis (45, 56). As seen previously, titan cells comprised approximately 21% of the total cryptococcal cell population in the lungs of mice infected with the H99 WT strain (Fig. 8C). Disruption of *MBS1* led to a significant decrease (12%, $P = 0.0015$) in titan cell production in mice infected with the *mbs1*Δ mutant strain. Restoring expression of *MBS1* in the *mbs1*Δ/*MBS1* complemented strain resulted in enhanced titan cell formation. These data suggest that Mbs1 is involved in titan cell formation and may affect interactions with the host by this mechanism.

A strong Th2 response to *C. neoformans* has been well characterized in mice; the response is nonprotective and does not promote clearance of the organism (10, 15). Dissemination from the lungs to the central nervous system (CNS) occurs readily during infection with highly virulent strains such as H99, resulting in cryptococcoma formation in the lungs and brains of infected animals (13). As seen in Fig. 8A, animals infected with the *mbs1*Δ mutant succumbed to the infection, even with the defects in virulence factor and titan cell production exhibited by this strain. Yet, animals infected with the *mbs1*Δ mutant never exhibited neurological symptoms and appeared instead to succumb to the pulmonary infection. One possible reason for this could be differences in the host immune response to the two organisms. To begin characterizing whether the host response to the *mbs1*Δ mutant strain contributed to pathogenicity, we examined lung and brain tissue sections at 21 days postinfection from animals infected with either the WT or *mbs1*Δ strain.

Extensive proliferation of *C. neoformans* was evident throughout the lung tissue from mice infected with the WT strain (Fig. 9A and C); only small areas at the periphery of the lung lobes remained uninfected. Large areas of lung parenchyma exhibited alveoli distended with organisms of various sizes, myriads of very small organisms, and various numbers of larger organisms (Fig. 9C). Scattered multifocal infiltrates of low numbers of polymorphonuclear leukocytes and/or foamy macrophages were found near bronchioles and blood vessels. Low to moderate numbers of lymphocytes were seen surrounding occasional blood vessels, bronchi, and bronchioles. The bronchial epithelium appeared to be undergoing mucinous metaplasia in severely affected areas (data not shown). Similar infections and host responses were observed with the *mbs1*Δ/*MBS1* complemented strain (data not shown).

Conversely, in lungs infected with the *mbs1*Δ mutant, a larger amount of the lung field was relatively intact, with only occasional organisms identified within alveoli (Fig. 9B). Areas in which organisms were present had very dense pulmonary consolidation with large numbers of foamy macrophages present, many of which contained cryptococci (Fig. 9D). These areas also had thickened alveolar septa with marked type 2 cell hyperplasia and mild fibroplasia. Other foci of organisms within the pulmonary parenchyma appeared to be surrounded by dense infiltrates of polymorphonuclear leukocytes, often with associated necrosis. These results suggest that the host response in the lungs to the *mbs1*Δ mutant is distinctly different from the response to the highly virulent H99 strain.

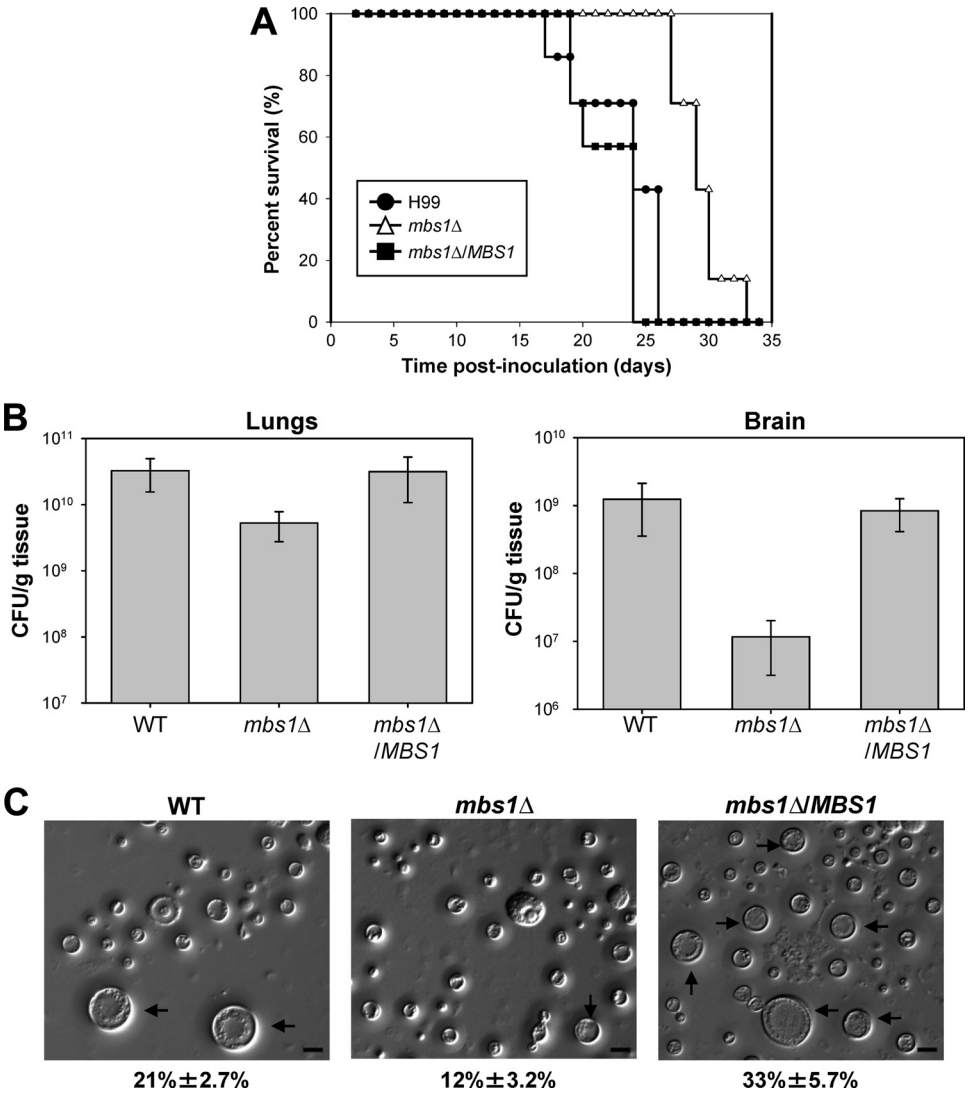

FIG 8 Mbs1 is required for virulence of *C. neoformans*. (A) Groups of A/J mice were infected with 5×10^4 cells of *MATα* WT (H99), *mbs1*Δ (YSB488), and *mbs1*Δ/*MBS1* complemented (YSB1195) strains by intranasal inhalation. Survival was monitored for 33 days postinfection. (B) A/J mice were infected as indicated for panel A. Fungal burden (CFU/g tissue) was determined by plating homogenates of lung or brain tissue onto YPD at 21 days postinfection. *P* values for lungs: 0.05 (WT versus *mbs1*Δ), 0.949 (*mbs1*Δ/*MBS1* versus WT), and 0.096 (*mbs1*Δ versus *mbs1*Δ/*MBS1*). *P* values for brains: 0.0747 (WT versus *mbs1*Δ), 0.5359 (WT versus *mbs1*Δ/*MBS1*), and 0.0302 (*mbs1*Δ/*MBS1* versus *mbs1*Δ). (C) Mice were infected with 5×10^6 cells of *MATα* WT (H99), *mbs1*Δ (YSB488), and *mbs1*Δ/*MBS1* complemented (YSB1195) strains by intranasal inhalation. Cells were obtained by bronchial alveolar lavage at 3 days postinfection, fixed in formaldehyde, and analyzed by microscopy for size and morphology. More than 300 cells per animal were examined. Representative images are shown. Numbers indicate the percent titan cell formation ± SD. *P* values in pairwise comparisons: 0.0112 (WT versus *mbs1*Δ), 0.0294 (WT versus *mbs1*Δ/*MBS1*), and 0.0015 (*mbs1*Δ versus *mbs1*Δ/*MBS1*). Black arrows, titan cells. Bars = 10 μm.

Because the *mbs1*Δ mutant-infected animals did not exhibit signs of neurological involvement, we analyzed brain sections to look for differences in pathology within the CNS. Brain sections from mice infected with the WT strain had multifocal aggregations of *Cryptococcus* within the parenchyma with no evidence of inflammation (Fig. 9E). Organisms were also visualized multifocally within the meninges and immediate submeningeal locations (data not shown). In these areas, occasional polymorphonuclear leukocytes, microglial cells, or lymphocytes were present, especially in perivascular locations. In contrast, brain sections from mice infected with the *mbs1*Δ mutant contained fewer foci of organisms. The infected areas had fewer identifiable organisms, and the foci were infiltrated by polymorphonuclear leukocytes, astrocytes, and glial cells (Fig. 9F). Marked pyogranulomatous to purely granulomatous inflammation was associated with cryptococci within the meninges and penetrated into the superficial cerebral cortex (data not shown). Small foci of necrosis were present within the parenchyma with what appeared to be degenerate neutrophilic debris and cryptococci within the necrotic center (Fig. 9F). To our knowledge, these types of cells have not been previously reported surrounding cryptococcomas within the brains of infected animals.

DISCUSSION

The present study investigates the genome-wide flucytosine-response regulatory mechanism in *C. neoformans* with connection

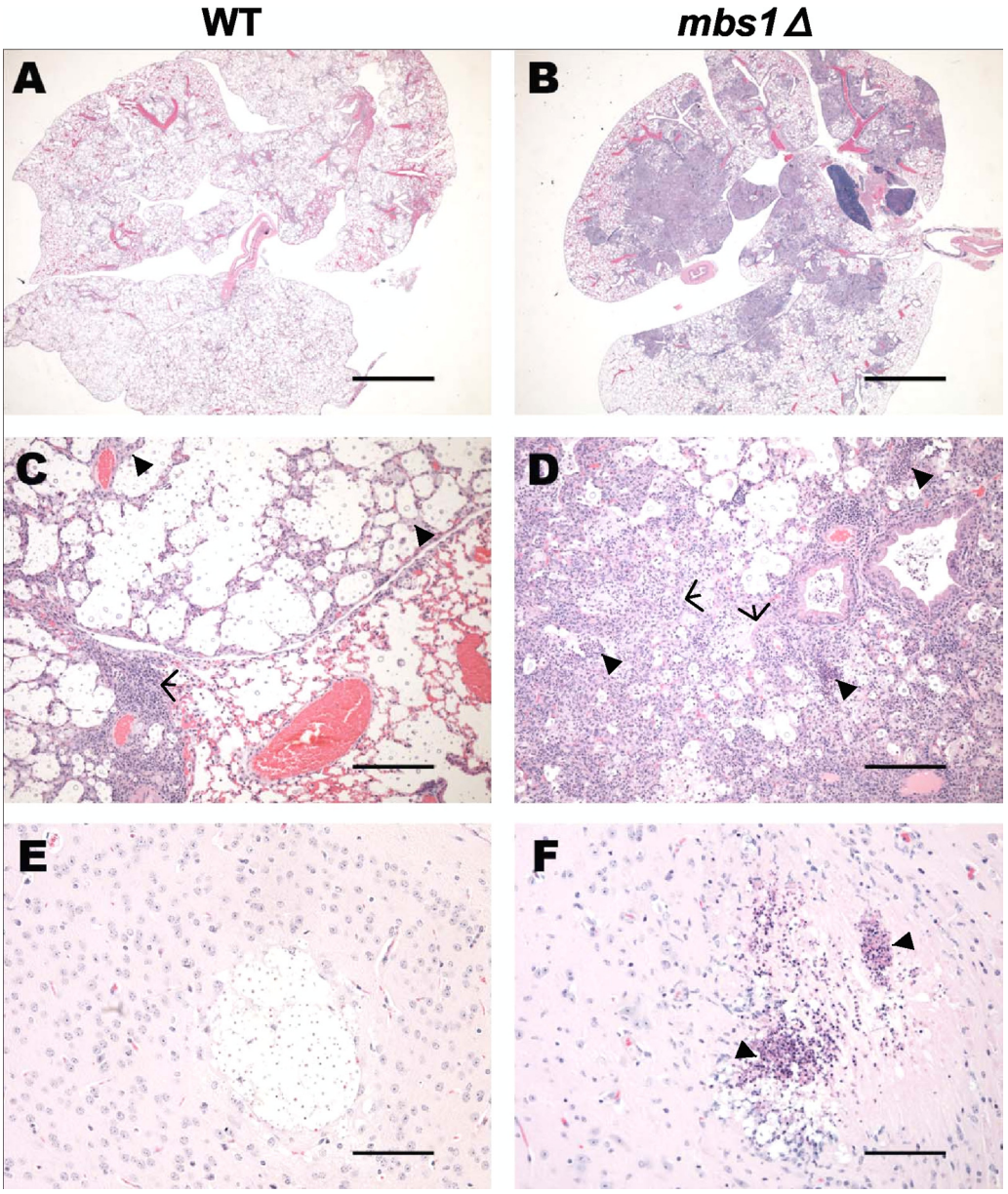

FIG 9 Mbs1 infection leads to an altered host immune response. Mice were infected with 5×10^4 cells of *MATα* WT (H99) and *mbs1*Δ (YSB488) strains by intranasal inhalation. Lungs sections were stained with H&E at 21 days postinfection. (A and C) WT-infected lungs. Arrowheads, foamy macrophages and/or polymorphonuclear cells; arrows, area of lymphocyte infiltration. (B and D) *mbs1*Δ mutant-infected lungs. Arrowheads, dense infiltrates of polymorphonuclear cells with and without necrosis; arrows, type 2 cell hyperplasia and mild fibroplasia. (E) WT-infected brain cryptococcoma. (F) *mbs1*Δ mutant-infected brain cryptococcoma. Arrowheads, neutrophilic debris and necrosis. Bars = 4 mm (A and B), 200 μm (C and D), and 100 μm (E and F).

to the two-component system and HOG signaling pathway, which is a first in the human meningitis-causing fungal pathogen. As a key discovery of this transcriptome analysis, we identified the *MBS1* gene, encoding an APSES-like transcription factor, whose expression is modulated upon flucytosine treatment. Both Tco2 and Hog1 repress basal expression levels of *MBS1*, whereas only Tco2 appeared to be involved in flucytosine-responsive induction of *MBS1*. APSES-like proteins have never been studied before in *C. neoformans*. Phenotypic analyses of *mbs1* deletion mutants revealed that Mbs1 plays pleiotropic functions in *C. neoformans*, including regulation of susceptibility to diverse antifungal drugs such as flucytosine, azole, and polyene drugs; ergosterol biosynthesis; cell membrane stability; genotoxic, oxidative, and salt stress responses; *in vitro* and *in vivo* morphological differentiation; virulence factor production; and virulence of the pathogen.

Flucytosine is one of the most widely used antifungal drugs for treatment of deadly cryptococcosis, although it is generally used in combination with AMB due to the tendency to develop drug resistance. Despite its importance, regulatory and resistance mechanisms for flucytosine are poorly understood in *C. neoformans* and have generally been assumed to be similar to those in *S. cerevisiae* and *C. albicans*. Several lines of evidence provided in this study indicate that *C. neoformans* has developed distinct defense mechanisms against flucytosine. First, the role of sensor histidine ki-

nases in flucytosine resistance has not been reported in any other organisms. In particular, Tco2 is a unique sensor histidine kinase observed only in *C. neoformans* which carries two response regulator and histidine kinase domains in a single polypeptide. Deletion of *TCO2* confers strong resistance to flucytosine in *C. neoformans*, whereas mutation of *TCO1* increases susceptibility to flucytosine, indicating that the pathogen employs the two-component system for modulating the flucytosine-response pathway. Second, flucytosine-responsive transcriptome patterns in *C. neoformans* were significantly different from those in *S. cerevisiae* (57). Among the 177 flucytosine-regulated genes in *C. neoformans*, none of them overlapped with those in *S. cerevisiae*, which strongly suggests that *C. neoformans* employs a distinct set of genes to respond to flucytosine. To further support this, a majority of the flucytosine-regulated genes in *C. neoformans* (118 out of 177, 67%) appeared to have no known functions in other fungi. Taken together, *C. neoformans* utilizes a unique defensive mechanism against flucytosine treatment.

Among the 59 evolutionarily conserved flucytosine-responsive genes, *STE14* (CNAG_01592.2), encoding the isoprenylcysteine carboxyl methyltransferase (ICMT), was the most highly upregulated (~16-fold) in the WT strain but not in the *tco1*Δ, *tco2*Δ, and *hog1*Δ mutants (Table 1). These data could be related to our previous finding showing that Ras1 promotes flucytosine resistance in *C. neoformans* (28). Ras1 undergoes two essential posttranslational modifications, palmitoylation and prenylation, which are required for proper cellular localization and function of the small GTPase protein (44). Nichols et al. (44) demonstrated that point mutation of a cysteine residue (C207A) in the CAAX motif causes abnormal cellular localization of Ras1, which subsequently abolishes its normal function, such as promoting growth at host physiological temperature, indicating that prenylation of the CAAX motif is essential for Ras1 in *C. neoformans*. Ste14 is required for prenylation of CAAX proteins by transferring a methyl group to the C-terminal prenylcysteine. The increased expression of the *STE14* ortholog may enhance or facilitate prenylation and membrane localization of Ras1 to the plasma membrane, affecting its resistance to flucytosine. This possibility is under investigation.

Among the flucytosine-regulated *C. neoformans* genes, the APSES-like Mbs1 transcription factor, homologous to the yeast Mbp1 and Swi4, which play redundant roles during the G_1/S transition in cell cycle progression (31), is most notable because no other APSES or APSES-like proteins have hitherto been characterized in the pathogen and their involvement in flucytosine resistance has not been reported in any other fungal species. On the basis of analysis of the *Cryptococcus* genome database, *Cryptococcus* does not appear to contain APSES proteins that are directly orthologous to other fungal APSES proteins. In addition to the Mbp1/Swi4 ortholog (CNAG_07464.2), *C. neoformans* possesses another APSES-like ortholog (CNAG_01438.2) which is also homologous to Mbp1 and Swi4. However, the yeast Swi6 shares higher sequence identity to CNAG_01438.2 than Mbp1 and Swi4. Unlike *S. cerevisiae* and *C. albicans*, it appears that *C. neoformans* contains a single nonessential Mbp1/Swi4-like protein (Mbs1). Our array results show that *SWI6* was not regulated in response to flucytosine (see Tables S4 and S5 in the supplemental material), indicating that Mbs1 may be involved in flucytosine response independently of cell cycle progression. Recently, Walsh et al. reported that expression of *RNR2*, which encodes ribonucleotide reductase, is induced by DNA-damaging agents, such as MMS, and is regulated by Mbp1 in *S. cerevisiae* (53). Therefore, it is possible that flucytosine treatment hampers DNA synthesis, which subsequently activates *RNR2* through the Mbs1 transcription factor.

Both the two-component system and the HOG pathway are likely to be the upstream signaling pathways for Mbs1, based on several observations made by this study. First, flucytosine-mediated induction of *MBS1* was not observed in the *tco2*Δ mutants in both DNA microarray and Northern blot/qRT-PCR analyses. In contrast, both basal and induced levels of *MBS1* were higher in the *hog1*Δ mutant than WT. Second, a number of phenotypes of the *mbs1*Δ mutant are closely related to those of the *tco2*Δ or *hog1*Δ mutants. For example, the phenotypes of the *mbs1*Δ mutant, including enhanced ergosterol production and increased sensitivity to a DNA-damaging agent (HU), membrane destabilizer (SDS), and high salt conditions, were very similar to those of the *hog1*Δ mutant. At this point, the exact Mbs1 regulatory mechanism in the two-component system and HOG pathways remains unknown. Whether Mbs1 is directly activated by Hog1 needs to be addressed in future studies. However, other HOG-independent signaling pathways are also likely to regulate Mbs1 because several phenotypes of the *mbs1*Δ mutant, such as extreme TBZ resistance and production of capsule and melanin, could not be explained only by signaling through the HOG pathway.

The role of APSES proteins in ergosterol biosynthesis has been reported in *C. albicans*, although its regulatory mechanism appears to be different from that of Mbs1 in *C. neoformans*. Deletion of *EFG1* diminishes cellular ergosterol content by decreasing expression levels of *ERG11* and enhances membrane fluidity and passive diffusion of drugs (47). Hence, the homozygous *efg1*Δ/*efg1*Δ mutant is more susceptible to both polyene and azole drugs than wild type (47). In contrast, our study revealed that the *mbs1*Δ mutant exhibited increased expression of *ERG11* and actual cellular ergosterol contents in *C. neoformans*. This phenotype of the *mbs1*Δ mutant is similar to that of the *hog1*Δ mutant. In *S. cerevisiae*, *ERG11* has been discovered to be SBF targets through chromatin immunoprecipitation-on-chip (ChIP-chip) analysis (25). Although the role of Swi4 in controlling ergosterol biosynthesis was not directly proven in *S. cerevisiae*, this finding and our data suggest that the Mbp1/Swi4 ortholog could be generally involved in ergosterol biosynthesis.

Supporting the role of Mbs1 in ergosterol biosynthesis, deletion of *MBS1* increased AMB susceptibility and azole drug resistance. Taken together with our previous data (29), it is highly likely that diverse signaling components of the two-component system and HOG pathway could be excellent antifungal targets for treatment of cryptococcosis, particularly when combined with other known antifungal agents. First, the potential inhibitors of Tco2, Ssk1, Ssk2, Pbs2, and Hog1 could have synergistic anticryptococcal effects with AMB. Among them, Tco2 and Ssk1 are involved in the two-component phosphorelay system, making them attractive targets for development of novel antifungal agents because the corresponding signaling components do not exist in humans. Second, the potential inhibitors of Tco1, Mbs1, and Ras1 could have synergistic anticryptococcal effects with flucytosine. Development of Mbs1-specific inhibitors could be particularly useful because they will show synergistic antifungal activity with AMB and flucytosine, the combination of which is currently most widely used for the initial therapeutic approach for treatment of

cryptococcosis. Furthermore, monotreatment with Mbs1-specific inhibitors could be also clinically useful since it was shown that Mbs1 inhibition alone debilitates virulence of *C. neoformans* (Fig. 8).

At this point, it is not clear how the production of two major virulence factors, capsule and melanin, and *in vivo* virulence of *C. neoformans* are controlled by Mbs1. The reduced virulence observed in the *mbs1*Δ mutant appears to be caused by multiple factors. Besides decreased production of capsule and melanin, inability to confer an appropriate cellular response against diverse environmental stresses and weak cell membrane stability with increased cellular ergosterol content could also contribute to reduced virulence of the *mbs1*Δ mutant. Furthermore, debilitated titan cell formation may render the *mbs1*Δ mutant more susceptible to phagocytosis, which could facilitate its clearance by the host immunological system. On the basis of our histopathology results, as well as the differences in morbidity and mortality observed in infected animals, it is clear that the host immune response to the *mbs1*Δ mutant is altered relative to a highly virulent strain such as H99. The pathology observed in the lungs of *mbs1*Δ mutant-infected mice appears to be similar to that reported previously in interleukin-4 (IL-4)/IL-13$^{-/-}$ mice infected with strain H99 (58), suggesting that infection with the *mbs1*Δ mutant strain may alter the host immune response to pulmonary infection. This altered immune response could explain the presence of numerous host immune cells within the brains of mice infected with the *mbs1*Δ mutant, specifically as it pertains to the presence of inflammatory cells not typically found in the brains of animals infected by *C. neoformans*.

In future studies, several aspects of the regulatory mechanism of Mbs1 need to be further addressed. First, in addition to Tco2 and Hog1, a full array of upstream signaling components modulating expression or activity of Mbs1 needs to be elucidated. Second, based on the pleiotropic roles of Mbs1, how the Mbs1-dependent signaling pathway is functionally and structurally connected to other signaling pathways in *C. neoformans* also needs to be clarified. It is possible that the Skn7 response regulator might be involved in functions of Mbs1 in regulation of some virulence factors, such as melanin and oxidative stress response. In *S. cerevisiae*, Skn7 physically interacts with Mbp1, but not with Swi4 or Swi6, via its coiled-coil domain and receiver domain and is directly associated with the G_1 transcriptional machinery (12). In *C. neoformans*, Skn7 controls melanin biosynthesis and Na^+ salt and oxidative stress adaptation (7). Therefore, functions of Mbs1 in melanin and oxidative stress response could be related to those of Skn7 in the pathogen. Potential molecular and genetic relationships between Mbs1 and Skn7 in *C. neoformans* need further investigation.

ACKNOWLEDGMENTS

We are grateful to Yin-Won Lee for sincere comments and encouragement. We also thank Young-Joon Ko for his technical assistance.

This work was supported by National Research Foundation of Korea grants (no. 2008-0061963, no. 2010-0029117) from MEST (to Y.-S.B). This work was also supported in part by RO1 grant AI50438-08 and R37 award AI39115-14 from the NIH/NIAID (to J.H.), RO1 grants AI080275, AI070152, and AI089244 from the NIH/NIAID (to K.N.), and grant DE017078 from the NIH (to T.C.W.).

REFERENCES

1. **Alspaugh JA, Perfect JR, Heitman J.** 1997. *Cryptococcus neoformans* mating and virulence are regulated by the G-protein α subunit GPA1 and cAMP. Genes Dev. **11**:3206–3217.
2. **Aramayo R, Peleg Y, Addison R, Metzenberg R.** 1996. Asm-1+, a *Neurospora crassa* gene related to transcriptional regulators of fungal development. Genetics **144**:991–1003.
3. **Baddley JW, Pappas PG.** 2005. Antifungal combination therapy: clinical potential. Drugs **65**:1461–1480.
4. **Baginski M, Czub J.** 2009. Amphotericin B and its new derivatives—mode of action. Curr. Drug Metab. **10**:459–469.
5. **Bahn YS, Hicks JK, Giles SS, Cox GM, Heitman J.** 2004. Adenylyl cyclase-associated protein AcaI regulates virulence and differentiation of *Cryptococcus neoformans* via the cyclic AMP-protein kinase A cascade. Eukaryot. Cell **3**:1476–1491.
6. **Bahn YS, Kojima K, Cox GM, Heitman J.** 2005. Specialization of the HOG pathway and its impact on differentiation and virulence of *Cryptococcus neoformans.* Mol. Biol. Cell **16**:2285–2300.
7. **Bahn YS, Kojima K, Cox GM, Heitman J.** 2006. A unique fungal two-component system regulates stress responses, drug sensitivity, sexual development, and virulence of *Cryptococcus neoformans.* Mol. Biol. Cell **17**:3122–3135.
8. **Bean JM, Siggia ED, Cross FR.** 2005. High functional overlap between MluI cell-cycle box binding factor and Swi4/6 cell-cycle box binding factor in the G_1/S transcriptional program in *Saccharomyces cerevisiae.* Genetics **171**:49–61.
9. **Black KE, Baden LR.** 2007. Fungal infections of the CNS: treatment strategies for the immunocompromised patient. CNS Drugs **21**:293–318.
10. **Blackstock R, Buchanan KL, Adesina AM, Murphy JW.** 1999. Differential regulation of immune responses by highly and weakly virulent *Cryptococcus neoformans* isolates. Infect. Immun. **67**:3601–3609.
11. **Block ER, Jennings AE, Bennett JE.** 1973. 5-Fluorocytosine resistance in *Cryptococcus neoformans.* Antimicrob. Agents Chemother. **3**:649–656.
12. **Bouquin N, Johnson AL, Morgan BA, Johnston LH.** 1999. Association of the cell cycle transcription factor Mbp1 with the Skn7 response regulator in budding yeast. Mol. Biol. Cell **10**:3389–3400.
13. **Carroll SF, Guillot L, Qureshi ST.** 2007. Mammalian model hosts of cryptococcal infection. Comp. Med. **57**:9–17.
14. **Chang YC, Bien CM, Lee H, Espenshade PJ, Kwon-Chung KJ.** 2007. Sre1p, a regulator of oxygen sensing and sterol homeostasis, is required for virulence in *Cryptococcus neoformans.* Mol. Microbiol. **64**:614–629.
15. **Chen GH, et al.** 2008. Inheritance of immune polarization patterns is linked to resistance versus susceptibility to *Cryptococcus neoformans* in a mouse model. Infect. Immun. **76**:2379–2391.
16. **Datta K, et al.** 2009. Spread of *Cryptococcus gattii* into Pacific Northwest region of the United States. Emerg. Infect. Dis. **15**:1185–1191.
17. **Davidson RC, et al.** 2002. A PCR-based strategy to generate integrative targeting alleles with large regions of homology. Microbiology **148**:2607–2615.
18. **Del Poeta M, Cruz MC, Cardenas ME, Perfect JR, Heitman J.** 2000. Synergistic antifungal activities of bafilomycin A(1), fluconazole, and the pneumocandin MK-0991/caspofungin acetate (L-743,873) with calcineurin inhibitors FK506 and L-685,818 against *Cryptococcus neoformans.* Antimicrob. Agents Chemother. **44**:739–746.
19. **Dutton JR, Johns S, Miller BL.** 1997. StuAp is a sequence-specific transcription factor that regulates developmental complexity in *Aspergillus nidulans.* EMBO J. **16**:5710–5721.
20. **Garcia-Pedrajas MD, Baeza-Montanez L, Gold SE.** 2010. Regulation of *Ustilago maydis* dimorphism, sporulation, and pathogenic development by a transcription factor with a highly conserved APSES domain. Mol. Plant Microbe Interact. **23**:211–222.
21. **Gimeno CJ, Fink GR.** 1994. Induction of pseudohyphal growth by overexpression of *PHD1*, a *Saccharomyces cerevisiae* gene related to transcriptional regulators of fungal development. Mol. Cell. Biol. **14**:2100–2112.
22. **Granger DL, Perfect JR, Durack DT.** 1985. Virulence of *Cryptococcus neoformans.* Regulation of capsule synthesis by carbon dioxide. J. Clin. Invest. **76**:508–516.
23. **Hossack JA, Rose AH.** 1976. Fragility of plasma membranes in *Saccharomyces cerevisiae* enriched with different sterols. J. Bacteriol. **127**:67–75.
24. **Idnurm A, et al.** 2005. Deciphering the model pathogenic fungus *Cryptococcus neoformans.* Nat. Rev. Microbiol. **3**:753–764.

25. **Iyer VR, et al.** 2001. Genomic binding sites of the yeast cell-cycle transcription factors SBF and MBF. Nature **409**:533–538.
26. **Jung KW, Kim SY, Okagaki LH, Nielsen K, Bahn YS.** 2011. Ste50 adaptor protein governs sexual differentiation of *Cryptococcus neoformans* via the pheromone-response MAPK signaling pathway. Fungal Genet. Biol. **48**:154–165.
27. **Jung WH, Hu G, Kuo W, Kronstad JW.** 2009. Role of ferroxidases in iron uptake and virulence of *Cryptococcus neoformans.* Eukaryot. Cell **8**:1511–1520.
28. **Kim MS, et al.** 2010. Comparative transcriptome analysis of the CO_2 sensing pathway via differential expression of carbonic anhydrase in *Cryptococcus neoformans.* Genetics **185**:1207–1219.
29. **Ko YJ, et al.** 2009. Remodeling of global transcription patterns of *Cryptococcus neoformans* genes mediated by the stress-activated HOG signaling pathways. Eukaryot. Cell **8**:1197–1217.
30. **Koc A, Wheeler LJ, Mathews CK, Merrill GF.** 2004. Hydroxyurea arrests DNA replication by a mechanism that preserves basal dNTP pools. J. Biol. Chem. **279**:223–230.
31. **Koch C, Moll T, Neuberg M, Ahorn H, Nasmyth K.** 1993. A role for the transcription factors Mbp1 and Swi4 in progression from G_1 to S phase. Science **261**:1551–1557.
32. **Kojima K, Bahn YS, Heitman J.** 2006. Calcineurin, Mpk1 and Hog1 MAPK pathways independently control fludioxonil antifungal sensitivity in *Cryptococcus neoformans.* Microbiology **152**:591–604.
33. **Lee JW, Ko YJ, Kim SY, Bahn YS.** 2011. Multiple roles of Ypd1 phosphotransfer protein in viability, stress response, and virulence factor regulation in *Cryptococcus neoformans.* Eukaryot. Cell **10**:998–1002.
34. **Lin X, Heitman J.** 2006. The biology of the *Cryptococcus neoformans* species complex. Annu. Rev. Microbiol. **60**:69–105.
35. **Livak KJ, Schmittgen TD.** 2001. Analysis of relative gene expression data using real-time quantitative PCR and the $2^{-\Delta\Delta CT}$ method. Methods **25**: 402–408.
36. **Lo HJ, et al.** 1997. Nonfilamentous *C. albicans* mutants are avirulent. Cell **90**:939–949.
37. **Lopez-Mirabal HR, Winther JR.** 2008. Redox characteristics of the eukaryotic cytosol. Biochim. Biophys. Acta **1783**:629–640.
38. **Lundin C, et al.** 2005. Methyl methanesulfonate (MMS) produces heat-labile DNA damage but no detectable in vivo DNA double-strand breaks. Nucleic Acids Res. **33**:3799–3811.
39. **Lupetti A, Nibbering PH, Campa M, Del Tacca M, Danesi R.** 2003. Molecular targeted treatments for fungal infections: the role of drug combinations. Trends Mol. Med. **9**:269–276.
40. **Maeng S, et al.** 2010. Comparative transcriptome analysis reveals novel roles of the Ras and cyclic AMP signaling pathways in environmental stress response and antifungal drug sensitivity in *Cryptococcus neoformans.* Eukaryot. Cell **9**:360–378.
41. **McLean-Bowen CA, Parks LW.** 1982. Effect of altered sterol composition on the osmotic behavior of sphaeroplasts and mitochondria of *Saccharomyces cerevisiae.* Lipids **17**:662–665.
42. **Miller KY, Toennis TM, Adams TH, Miller BL.** 1991. Isolation and transcriptional characterization of a morphological modifier: the *Aspergillus nidulans* stunted (stuA) gene. Mol. Gen. Genet. **227**:285–292.
43. **Miller KY, Wu J, Miller BL.** 1992. StuA is required for cell pattern formation in *Aspergillus.* Genes Dev. **6**:1770–1782.
44. **Nichols CB, Ferreyra J, Ballou ER, Alspaugh JA.** 2009. Subcellular localization directs signaling specificity of the *Cryptococcus neoformans* Ras1 protein. Eukaryot. Cell **8**:181–189.
45. **Okagaki LH, et al.** 2010. Cryptococcal cell morphology affects host cell interactions and pathogenicity. PLoS Pathog. **6**:e1000953.
46. **Park BJ, et al.** 2009. Estimation of the current global burden of cryptococcal meningitis among persons living with HIV/AIDS. AIDS **23**: 525–530.
47. **Prasad T, et al.** 2010. Morphogenic regulator *EFG1* affects the drug susceptibilities of pathogenic *Candida albicans.* FEMS Yeast Res. **10**: 587–596.
48. **Ramirez-Zavala B, Dominguez A.** 2008. Evolution and phylogenetic relationships of APSES proteins from Hemiascomycetes. FEMS Yeast Res. **8**:511–519.
49. **Segal BH, Steinbach WJ.** 2007. Combination antifungals: an update. Expert Rev. Anti Infect. Ther. **5**:883–892.
50. **Sloan D, Dlamini S, Paul N, Dedicoat M.** 2008. Treatment of acute cryptococcal meningitis in HIV infected adults, with an emphasis on resource-limited settings. Cochrane Database Syst. Rev. **4**:CD005647.
51. **Stoldt VR, Sonneborn A, Leuker CE, Ernst JF.** 1997. Efg1p, an essential regulator of morphogenesis of the human pathogen *Candida albicans*, is a member of a conserved class of bHLH proteins regulating morphogenetic processes in fungi. EMBO J. **16**:1982–1991.
52. **Vermes A, Guchelaar HJ, Dankert J.** 2000. Flucytosine: a review of its pharmacology, clinical indications, pharmacokinetics, toxicity and drug interactions. J. Antimicrob. Chemother. **46**:171–179.
53. **Walsh L, et al.** 2002. DNA-damage induction of *RAD54* can be regulated independently of the *RAD9*- and *DDC1*-dependent checkpoints that regulate *RNR2.* Curr. Genet. **41**:232–240.
54. **Ward MP, Gimeno CJ, Fink GR, Garrett S.** 1995. *SOK2* may regulate cyclic AMP-dependent protein kinase-stimulated growth and pseudohyphal development by repressing transcription. Mol. Cell. Biol. **15**: 6854–6863.
55. **Whelan WL.** 1987. The genetic basis of resistance to 5-fluorocytosine in *Candida* species and *Cryptococcus neoformans.* Crit. Rev. Microbiol. **15**: 45–56.
56. **Zaragoza O, et al.** 2010. Fungal cell gigantism during mammalian infection. PLoS Pathog. **6**:e1000945.
57. **Zhang L, Zhang Y, Zhou Y, Zhao Y, Cheng J.** 2002. Expression profiling of the response of *Saccharomyces cerevisiae* to 5-fluorocytosine using a DNA microarray. Int. J. Antimicrob. Agents **20**:444–450.
58. **Zhang Y, et al.** 2009. Robust Th1 and Th17 immunity supports pulmonary clearance but cannot prevent systemic dissemination of highly virulent *Cryptococcus neoformans* H99. Am. J. Pathol. **175**:2489–2500.